COMPUTATION OF UNSTEADY MOMENTUM AND HEAT TRANSFER FROM A FIXED CIRCULAR CYLINDER IN LAMINAR FLOW

László Baranyi

Department of Fuid and Heat Engineering, University of Miskolc
3515 Miskolc - Egyetemváros, Hungary
`arambl@gold.uni-miskolc.hu`

Abstract. This paper presents a finite difference solution for 2D, low Reynolds number, unsteady flow around and heat transfer from a stationary circular cylinder placed in a uniform flow. The fluid is assumed to be incompressible and of constant property. The governing equations are the Navier-Stokes equations, the continuity equation, a Poisson equation for pressure and the energy equation. The temperature of the cylinder wall is kept constant and the viscous energy dissipation term is neglected in the energy equation. The computed Strouhal numbers, time-mean drag and base pressure coefficients, as well as the average Nusselt numbers compare well with existing experimental results.

1. Introduction

Investigating flow around a single circular cylinder has been the objective of a huge number of researchers, through experimental, theoretical, and numerical approaches to the problem. Despite the simple geometry, the problem is extremely complex and remains an intriguing one, and one with many applications. Knowledge of flow patterns around bluff bodies is important in the design of structures such as smokestacks, skyscrapers, or bridges. Long slender structures in wind are often subjected to large amplitude oscillation due to alternating vortex shedding, sometimes causing collapse of the structure. The same vortex shedding causes noisy operation of heat exchangers, as the pipes of the heat exchanger vibrate. These are some of the hydrodynamic aspects; another aspect of importance is the heat transfer to and from the fluid. Heat exchangers, hot wire anemometers, and cooling towers are some examples in which heat transfer is central; heat transfer between structures and the outside air is also affected by vortex shedding.

Because of the practical importance of this problem, there are numerous studies dealing with flow past cylinders that are fixed, oscillating, rotating, or in orbital motion. Among these, the fixed cylinder is usually the starting point of investigations, because it is relatively simple to carry out experiments on, and thus also for numerical studies, comparison with experimental data is possible to confirm validity of the computer method used. Roshko [1], Norberg [2], and Bearman [3] are among those who have provided invaluable experimental data on flow around a fixed cylinder. Computations on the same problem have been performed by many researchers, including Kawamura and Kuwahara [4], Braza et al. [5], and Karniadakis and Triantafyllou [6].

Heat transfer has been investigated for fixed heated cylinders in a uniform stream at low Reynolds numbers with a focus on application to hot wire anemometry by investigators such as Lange et al. [7]. In their case, computations were carried out at extremely low Reynolds numbers as well, and they claim to have identified the critical Reynolds number where vortex shedding starts at $Re=45.9$.

Mahfouz and Badr [8] carried out a numerical study on a fixed and a rotationally oscillating cylinder between $Re=40$ and 200. They attempted to investigate the possibility of controlling heat transfer using a rotationally oscillating cylinder, and found that heat transfer was appreciably enhanced in the lock-in range, and the effect of the oscillation on heat transfer was insignificant for non-lock-in cases.

In the author's earlier studies, computations were carried out for the flow around a fixed circular cylinder at different Reynolds numbers, from $Re=10$ to 1000, and up to $Re=180$ for an oscillating cylinder (e.g. Baranyi and Shirakashi, [9]), and good agreement was obtained with experimental data for the variation of Strouhal number and time mean drag coefficient with Reynolds number. Here, further features of flow are investigated for a fixed cylinder and compared with experimental data. The base pressure coefficient, which influences the near-wake structure, is investigated and compared with the experimental data of Roshko [10]. Also, the author's computational results were compared with those of Sherwin's unpublished computations carried out by a different method, for the time mean drag coefficient, Strouhal number, and the root-mean square (rms) values of lift and drag coefficients at several Reynolds numbers up to $Re=140$. These comparisons were used to further validate the computer method used. Based on the results, the method was extended to investigate the heat transfer from a heated cylinder in which the temperature is kept constant and the fluid is assumed to be constant property incompressible fluid.

2. Governing equations

When deriving the basic equations constant property incompressible fluid flow is assumed. The governing equations in non-dimensional forms are the two components of the Navier-Stokes equations, the equation of continuity, a Poisson equation for pressure p, and the energy equation:

$$\frac{\partial u}{\partial t} + u\frac{\partial u}{\partial x} + v\frac{\partial u}{\partial y} = -\frac{\partial p}{\partial x} + \frac{1}{\text{Re}}\left(\frac{\partial^2 u}{\partial x^2} + \frac{\partial^2 u}{\partial y^2}\right); \qquad (2.1)$$

$$\frac{\partial v}{\partial t} + u\frac{\partial v}{\partial x} + v\frac{\partial v}{\partial y} = -\frac{\partial p}{\partial y} + \frac{1}{\text{Re}}\left(\frac{\partial^2 v}{\partial x^2} + \frac{\partial^2 v}{\partial y^2}\right); \tag{2.2}$$

$$D = \frac{\partial u}{\partial x} + \frac{\partial v}{\partial y} = 0; \tag{2.3}$$

$$\nabla^2 p = \frac{\partial^2 p}{\partial x^2} + \frac{\partial^2 p}{\partial y^2} = 2\left[\frac{\partial u}{\partial x}\frac{\partial v}{\partial y} - \frac{\partial u}{\partial y}\frac{\partial v}{\partial x}\right] - \frac{\partial D}{\partial t}; \tag{2.4}$$

$$\frac{\partial T}{\partial t} + u\frac{\partial T}{\partial x} + v\frac{\partial T}{\partial y} = \frac{1}{\text{RePr}}\left(\frac{\partial^2 T}{\partial x^2} + \frac{\partial^2 T}{\partial y^2}\right) + \frac{E}{\text{Re}}\Phi. \tag{2.5}$$

In these equations quantities are made dimensionless by using a length scale L chosen to be the diameter of the cylinder d, velocity scale U which is the free stream velocity, density ρ, kinematic viscosity υ, specific heat at constant pressure c_p, and the temperature difference between the cylinder surface (w) and the outer boundary (∞) of the computational domain $\left(\tilde{T}_w - \tilde{T}_\infty\right)$. In these equations x,y are Cartesian coordinates, u,v are velocities in x,y directions, p is pressure, D is dilation, T is dimensionless fluid temperature defined by $T = \left(\tilde{T} - \tilde{T}_\infty\right)/\left(\tilde{T}_w - \tilde{T}_\infty\right)$, where $\tilde{T}$ is the dimensional temperature, Re is the Reynolds number defined by $Re = Ud/\upsilon$, Pr is the Prandtl number $Pr = \rho\upsilon c_p/k$, where k is the thermal conductivity of the fluid, E is Eckert number defined by $E = U^2/\left[c_p\left(\tilde{T}_w - \tilde{T}_\infty\right)\right]$. The gravity force is included in the pressure terms in equations (2.1) and (2.2). Φ in equation (2.5) is the viscous energy dissipation function

$$\Phi = 2\left[\left(\frac{\partial u}{\partial x}\right)^2 + \left(\frac{\partial v}{\partial y}\right)^2\right] + \left(\frac{\partial u}{\partial y} + \frac{\partial v}{\partial x}\right)^2. \tag{2.6}$$

At low Reynolds numbers, as in this study, the viscous dissipation function can be neglected. Although the dilation D is zero by continuity (2.3), it is advisable to retain the term $\partial D/\partial t$ to avoid computational instability (Harlow and Welch, [11]).

Boundary conditions:

(R_1: cylinder surface)

$$u = v = 0 ;$$

$$\frac{\partial p}{\partial n} = \frac{1}{Re}\nabla^2 v_n;$$

$$T_1 = 1.$$

(R_2: undisturbed domain)

$$u = u_{pot}; \quad v = v_{pot};$$

$$\frac{\partial p}{\partial n} = \left(\frac{\partial p}{\partial n}\right)_{pot};$$

$$T_2 = 0.$$

Here subscript pot stands for potential flow and n denotes the outer normal along the cylinder.

The heat transfer rate per unit area from the cylinder wall to the fluid can be obtained from the temperature distribution and may be described as

$$\dot{q}_w = -k_w \left(\frac{\partial \tilde{T}}{\partial \tilde{r}} \right)_w ,$$ (2.7)

where $\tilde{T}$ and $\tilde{r}$ are the dimensional temperature and radius, k_w is the thermal conductivity of the fluid at cylinder temperature, and the subscript w indicates that the temperature gradient in the radial direction is evaluated at the cylinder wall. In this study constant property fluid is considered so the thermal conductivity of the fluid k is assumed to be constant, hence $k \cong k_w$. Engineers and technicians working in this field need an expression based on measurable quantities such as

$$\dot{q}_w = h \left(\tilde{T}_w - \tilde{T}_\infty \right) ,$$ (2.8)

where h is the heat transfer coefficient. By introducing dimensionless quantities the Nusselt number Nu can be obtained as

$$Nu = \frac{hd}{k} = - \left(\frac{\partial T}{\partial R} \right)_w ,$$ (2.9)

where T and R are the dimensionless temperature and radius. The temperature gradient in the fluid should be evaluated on the cylinder surface.

3. **Transformation from the physical plane to the computational plane**

We use a boundary-fitted coordinate system, hence boundary conditions can be imposed accurately. In this way interpolation leading to poor solutions can be avoided.
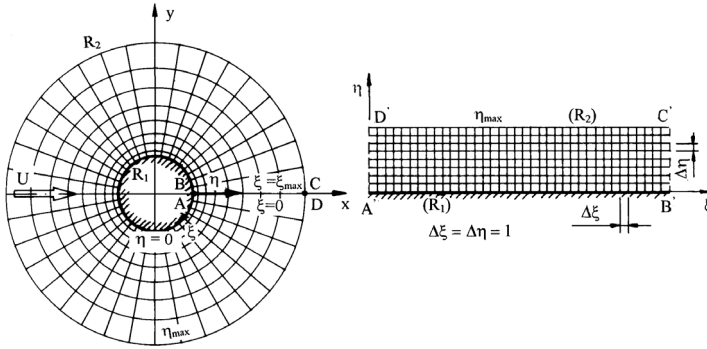

Figure 1. Physical and computational planes

A unique, single-valued relationship between the coordinates on the computational domain (ξ , η , τ) and the physical coordinates (x, y, t) (see Figure 1) can be written

as

$$x(\xi, \eta) = R(\eta) \cos[g(\xi)]; \quad y(\xi, \eta) = -R(\eta) \sin[g(\xi)]; \quad t = \tau, \qquad (2.10)$$

where the dimensionless radius

$$R(\eta) = R_1 \exp[f(\eta)]. \qquad (2.11)$$

This choice of the structure of the mapping function automatically assures that the obtained grid is orthogonal on the physical plane for arbitrary functions $f(\eta)$ and $g(\xi)$. In this study the following linear mapping functions were used

$$g(\xi) = 2\pi \frac{\xi}{\xi_{\max}}; \quad f(\eta) = \frac{\eta}{\eta_{\max}} \log\left(\frac{R_2}{R_1}\right), \qquad (2.12)$$

where subscript *max* refers to maximum value. Using mapping functions (2.12) cylindrical coordinates with logarithmically spaced radial cells are obtained on the physical plane, providing a fine grid scale near the cylinder wall and a coarse grid in the far field. Transformations (2.10)-(2.12) are single valued since in this case Jacobian J

$$J = y_\eta x_\xi - y_\xi x_\eta = \frac{2\pi \log\left(\frac{R_2}{R_1}\right)}{\xi_{\max}\eta_{\max}} R(\eta) \qquad (2.13)$$

is non-vanishing, positive for an arbitrary value of η in the computational domain. In equation (2.13) subscripts ξ and η denote differentiation. After having chosen the transformations between the physical and computational domains, the governing equations can also be transformed by variables used in the computational domain.

The x and y components of the transformed Navier-Stokes equations are

$$\frac{\partial u}{\partial \tau} + \frac{1}{J}\left(u\frac{\partial y}{\partial \eta} - v\frac{\partial x}{\partial \eta}\right)\frac{\partial u}{\partial \xi} + \frac{1}{J}\left(v\frac{\partial x}{\partial \xi} - u\frac{\partial y}{\partial \xi}\right)\frac{\partial u}{\partial \eta} =$$
$$-\frac{1}{J}\left(\frac{\partial y}{\partial \eta}\frac{\partial p}{\partial \xi} - \frac{\partial y}{\partial \xi}\frac{\partial p}{\partial \eta}\right) + \frac{1}{ReJ^2}\left(g_{22}\frac{\partial^2 u}{\partial \xi^2} + g_{11}\frac{\partial^2 u}{\partial \eta^2}\right); \qquad (2.14)$$

$$\frac{\partial v}{\partial \tau} + \frac{1}{J}\left(u\frac{\partial y}{\partial \eta} - v\frac{\partial x}{\partial \eta}\right)\frac{\partial v}{\partial \xi} + \frac{1}{J}\left(v\frac{\partial x}{\partial \xi} - u\frac{\partial y}{\partial \xi}\right)\frac{\partial v}{\partial \eta} =$$
$$-\frac{1}{J}\left(\frac{\partial x}{\partial \xi}\frac{\partial p}{\partial \eta} - \frac{\partial x}{\partial \eta}\frac{\partial p}{\partial \xi}\right) + \frac{1}{ReJ^2}\left(g_{22}\frac{\partial^2 v}{\partial \xi^2} + g_{11}\frac{\partial^2 v}{\partial \eta^2}\right). \qquad (2.15)$$

Dilation D transforms as

$$D = \frac{1}{J}\left(\frac{\partial y}{\partial \eta}\frac{\partial u}{\partial \xi} - \frac{\partial y}{\partial \xi}\frac{\partial u}{\partial \eta} + \frac{\partial x}{\partial \xi}\frac{\partial v}{\partial \eta} - \frac{\partial x}{\partial \eta}\frac{\partial v}{\partial \xi}\right) = 0. \qquad (2.16)$$

The Poisson equation for pressure will have the form

$$g_{22}\frac{\partial^2 p}{\partial \xi^2} + g_{11}\frac{\partial^2 p}{\partial \eta^2} = 2J\left(\frac{\partial u}{\partial \xi}\frac{\partial v}{\partial \eta} - \frac{\partial u}{\partial \eta}\frac{\partial v}{\partial \xi}\right) - J^2\frac{\partial D}{\partial \tau}. \qquad (2.17)$$

The energy equation by neglecting the viscous dissipation transforms as

$$\frac{\partial T}{\partial \tau} + \frac{1}{J}\left(u\frac{\partial y}{\partial \eta} - v\frac{\partial x}{\partial \eta}\right)\frac{\partial T}{\partial \xi} + \frac{1}{J}\left(v\frac{\partial x}{\partial \xi} - u\frac{\partial y}{\partial \xi}\right)\frac{\partial T}{\partial \eta} = \frac{1}{RePrJ^2}\left(g_{22}\frac{\partial^2 T}{\partial \xi^2} + g_{11}\frac{\partial^2 T}{\partial \eta^2}\right).$$
$$(2.18)$$

Boundary conditions for pressure will be transformed as

$$R = R_1 : \frac{\partial p}{\partial \eta} = \frac{g_{11}}{Re\, J^2} \left(\frac{\partial x}{\partial \eta} \frac{\partial^2 u}{\partial \eta^2} + \frac{\partial y}{\partial \eta} \frac{\partial^2 v}{\partial \eta^2} \right); \qquad (2.19)$$

$$R = R_2 : \frac{\partial p}{\partial \eta} \cong \left(\frac{\partial p}{\partial n} \right)_{pot}. \qquad (2.20)$$

In these equations the elements of the metric tensor will have the form

$$g_{11} = \left(\frac{\partial x}{\partial \xi} \right)^2 + \left(\frac{\partial y}{\partial \xi} \right)^2; \quad g_{22} = \left(\frac{\partial x}{\partial \eta} \right)^2 + \left(\frac{\partial y}{\partial \eta} \right)^2. \qquad (2.21)$$

The choice of transformations (2.10)-(2.12) renders the off-diagonal elements of the metric tensor zero, i.e., $g_{12} = g_{21} = 0$. That is the reason why the mixed second derivatives are missing from the Laplacian terms in equations (2.14), (2.15), (2.17)-(2.19). The transformation also ensures that the coefficients of the first order derivatives in the Laplacian terms in the above equations are zero (Fletcher, [12]). Since the mapping is given by elementary functions, the metric parameters and coordinate derivatives can be computed from closed forms, hence numerical differentiation leading to numerical errors can be avoided.

The grid aspect ratio AR [12], i.e., the ratio of the two sides of an elementary rectangle on the physical plane (see Figure 1), will have the form

$$AR = \sqrt{\frac{g_{22}}{g_{11}}} = \frac{f_\eta}{g_\xi} = \frac{\xi_{\max} \log (R_2/R_1)}{2\pi \eta_{\max}}. \qquad (2.22)$$

It can be seen from equation (2.22) that the grid aspect ratio is constant over the whole computational domain. By choosing the number of grid points in the ξ and η directions properly, this constant can be set to unity resulting in conformal transformation [12].

4. Numerical method applied and computational results

4.1. **Computational method.** The author developed a computer code which is applicable to the computation of flow around a fixed or oscillating cylinder, or a cylinder in orbital motion. This code calculates the velocity, pressure, and time histories of lift and drag coefficients. Several other quantities are calculated, including the vorticity distribution, stream function, the location of the front stagnation point, and the lower and upper separation points changing with time. The code has recently been extended to compute the heat transfer between a heated cylinder and the fluid flowing around it.

The transformed governing equations are solved by the finite difference method. The time derivatives in the transformed Navier-Stokes equations (2.14), (2.15) and in energy equation (2.18) are approximated by forward differences. Fourth order central difference scheme is used for the diffusion terms and the pressure derivatives. The widely used modified third order upwind scheme proposed by Kawamura and

Kuwahara [4] proved to be successful in handling the convective terms in the Navier-Stokes and energy equations.

The equations of motion and equation of energy are integrated explicitly giving the velocity and temperature distributions at every time step. In the knowledge of the velocity distribution in an arbitrary time step, the pressure is calculated from equation (2.17) by using the successive over-relaxation method (SOR). Dilation D is chosen to be zero at every time step. The pressure on the cylinder surface is calculated by the third order formula at every time step, shear stress on the cylinder surface is derived from the velocity distribution, and from the pressure and the shear stress we can derive the time histories of lift and drag coefficients. The non-dimensional vortex shedding frequency, Strouhal number St can be determined from the location of the spectrum peak of FFT, when applied to the oscillating lift coefficient or other oscillating signals.

The dimensionless heat transfer coefficient or local Nusselt number Nu is obtained at every time step by using the temperature distribution

$$Nu\left(\varphi,t\right) = \frac{hd}{k} = -\left(\frac{\partial T}{\partial R}\right)_w = -\left(\frac{\partial T}{\partial \eta}\right)_{\eta=0}\left(\frac{d\eta}{dR}\right)_{\eta=0} = -\frac{1}{R_1 f'\left(\eta=0\right)}\left(\frac{\partial T}{\partial \eta}\right)_{\eta=0}$$
(2.23)

where $f'\left(\eta\right)$ means the first derivative of f with respect to η, and φ is the polar angle measured along the periphery of the cylinder. The average Nusselt number $Nu\left(t\right)$ is obtained as

$$Nu\left(t\right) = \frac{1}{2\pi}\int_0^{2\pi} Nu\left(\varphi,t\right)d\varphi.$$

The time averaged Nusselt number $\overline{Nu}$ can also be obtained by taking the average of $Nu\left(t\right)$ over a time period taken after reaching the quasi-steady state and covering more than one cycle.

The computational grid used is 241x131 O-mesh. The diameter of the outer boundary of computation is $30d$, where $d = 2R_1$ is the cylinder diameter. Non-dimensional time steps used were usually 0.001 and 0.0005.

4.2. **Momentum transfer.** Previous studies by the author have focused upon the computation of momentum transfer between a uniform fluid flow and a single circular cylinder, either fixed or oscillating. Good agreement was obtained for fixed cylinders against experimental results for Strouhal number and mean drag coefficient versus Reynolds number [9]. Computations for oscillating cylinders were carried out to determine the amplitude threshold curve for locked-in vortex shedding due to crossflow cylinder oscillation [9].

A very important feature of momentum transfer is the base pressure coefficient. In Figure 2 time-mean values of the base pressure coefficients $\overline{C}_{pb}$, or the non-dimensional pressure measured at the farthest downstream point of the cylinder are compared with the experimental results of Roshko [10]. Agreement was good, but note that a discrepancy emerges at $Re=180$. This is fairly consistent with the findings of Williamson

[13] that flow becomes unstable and 3-D effects begin to appear above $Re=160$. This instability was accurately predicted by the computational code. Also shown in Figure 2 are the computed *rms* values of the base pressure C_{pbrms}. Below $Re=60$, this value is very small, which is in agreement with experimental findings that vortex shedding begins between $Re=40$ and 50 [3] or, as mentioned earlier, the value of 45.9 given in [7].
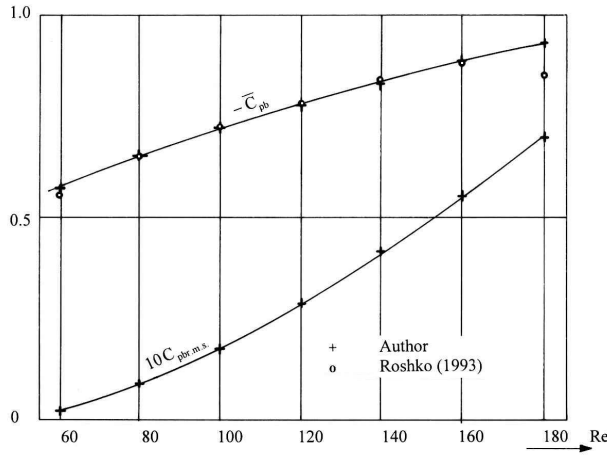
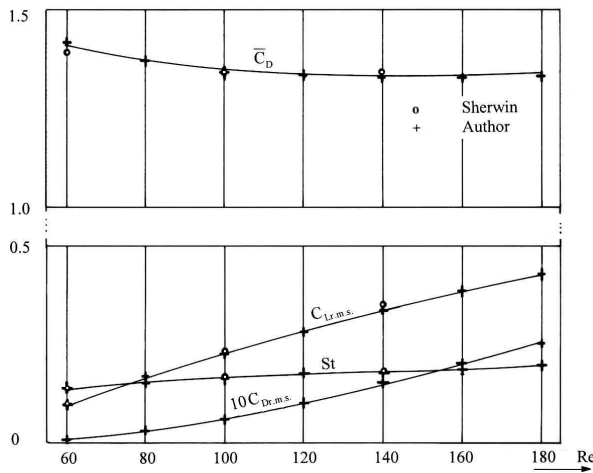Figure 2. Comparison of base pressures

Figure 3. Computational results for fixed cylinder with comparisons

To further determine momentum characteristics of flow, computations of the time-mean value and root-mean-square (*rms*) value of drag coefficients ($\overline{C}_D$ and C_{Drms}) and *rms* value of lift coefficient (C_{Lrms}) were made for a fixed cylinder at different Reynolds numbers. These and the non-dimensional vortex shedding frequency St

are shown in Figure 3, with comparisons with the unpublished computational results of S. Sherwin (Imperial College of Science, Technology and Medicine, using spectral element method) for $Re=60$, 100, and 140. As can be seen, the agreement is quite good.

4.3. **Heat transfer.** The cylinder surface is given a constant temperature, and the temperature of the fluid flowing around it is below the cylinder temperature, meaning that heat is transferred from the cylinder surface in the fluid. To keep a constant temperature, the cylinder is heated (as is the case with hot wire anemometer). Here, it is assumed that the temperature difference is not large enough to influence the properties of the fluid, and a constant property fluid was assumed in this study.
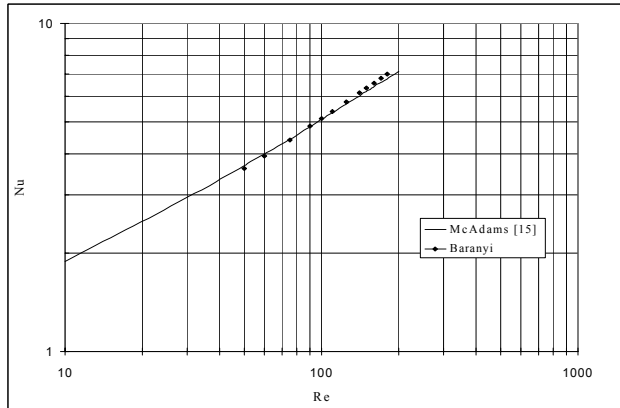

Figure 4. Measured and calculated time-averaged Nusselt number versus Reynolds number

Computations were carried out for fixed cylinders from $Re=50$ to 180, bearing in mind the fact that three-dimensional instability begins to occur at around $Re=160$, [13]. Figure 4 shows the author's computational results for time-averaged Nusselt numbers for different Reynolds numbers up to $Re=180$, and experimentally obtained time-averaged Nusselt number $\overline{Nu}$ for heating of air flowing across a single circular cylinder, versus Reynolds number, from Özisik [14] and McAdams [15]. As can be seen, the agreement is quite good, and possibly better than it appears in Figure 4. This is because the solid line is only a small part of a regression curve placed on experimentally measured values over an extremely wide Reynolds number domain, and the real measured values in the domain under consideration are above the regression curve itself, as are the computational results.

Computational results for which heat transfer has also been calculated are summarized in Table 1, as a function of Reynolds number. Strouhal number, time-mean values and rms values of the lift and drag coefficients, base pressure coefficient, and Nusselt number are given, with the exception of the time-mean value of the lift coefficient, which is zero. Note that values starting at $Re=160$ may be influenced by three-dimensional instability. It was found that Strouhal number derived from the

spectrum of the lift coefficient and that from the spectra of any other oscillating signal (C_D, C_{pb}, Nu) were somewhat different for Re=160 and above, and the averaged values for St are given in Table 1. This code predicts that the three-dimensional instability begins around Re=160.

Table 1. Effect of Re on momentum and heat transfer

Re	St	$\overline{C}_D$	$-\overline{C}_{pb}$	$\overline{Nu}$	C_{Lrms}	C_{Drms}	C_{pbrms}	Nu_{rms}
50	0.125	1.451	0.518	3.609	0.032	0.0001	0.0009	0.00004
60	0.137	1.419	0.574	3.950	0.093	0.0007	0.0022	0.0003
75	0.152	1.381	0.636	4.421	0.152	0.0024	0.0069	0.0008
90	0.163	1.357	0.687	4.856	0.199	0.0046	0.0129	0.0012
100	0.163	1.346	0.718	5.132	0.228	0.0064	0.0174	0.0014
110	0.171	1.338	0.747	5.396	0.256	0.0084	0.0226	0.0018
125	0.176	1.331	0.789	5.776	0.297	0.0117	0.0315	0.0027
140	0.179	1.325	0.830	6.136	0.337	0.0153	0.0413	0.0041
150	0.185	1.329	0.857	6.367	0.363	0.0178	0.0481	0.0056
160	0.188	1.330	0.883	6.590	0.388	0.0203	0.0552	0.0074
170	0.192	1.332	0.908	6.807	0.412	0.0229	0.0623	0.0094
180	0.195	1.334	0.933	7.018	0.435	0.0256	0.0696	0.0118

The rms values of the Nusselt number are shown in Figure 5. As can be seen, the amplitude of oscillation with time in the Nusselt number increases pronouncedly with increasing Reynolds number. This means that vortex shedding has an increased effect on heat transfer at larger Reynolds numbers.
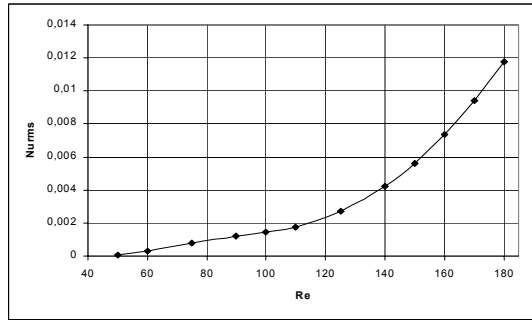

Figure 5. Root-mean-square value of Nusselt number versus Reynolds number

The time-history of the average Nusselt number Nu is shown for Re=150 in Figure 6. In the case of a fixed cylinder, the establishment of a quasi-steady state of vortex shedding takes a relatively long time. The frequency of oscillation in the Nusselt number is the same as the frequency of oscillation for the drag coefficient, while the frequency of oscillation of the lift coefficient is half that of Nu and the drag coefficient. This can be seen by taking the fast Fourier transform (FFT) of these three signals. Thus, in the case of the lift coefficient, one cycle consists of two vortices shed (clockwise

on the upper and counter-clockwise on the lower side), while for the drag coefficient and heat transfer, the shedding of a single vortex constitutes one cycle.
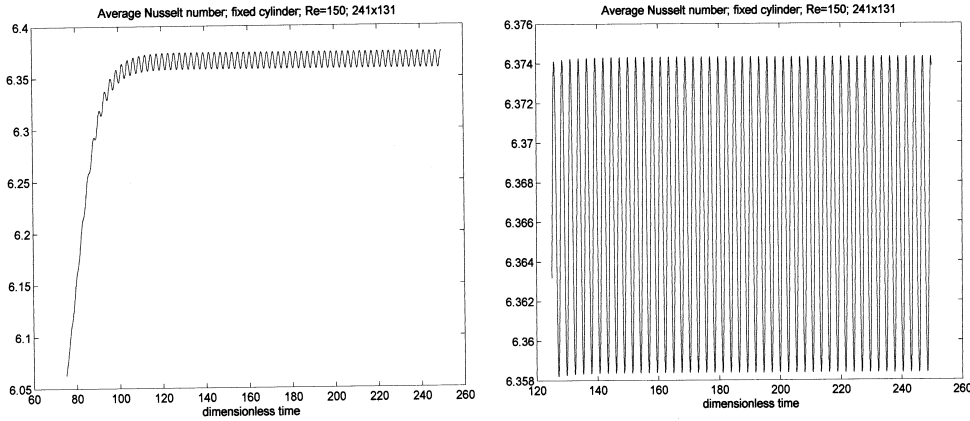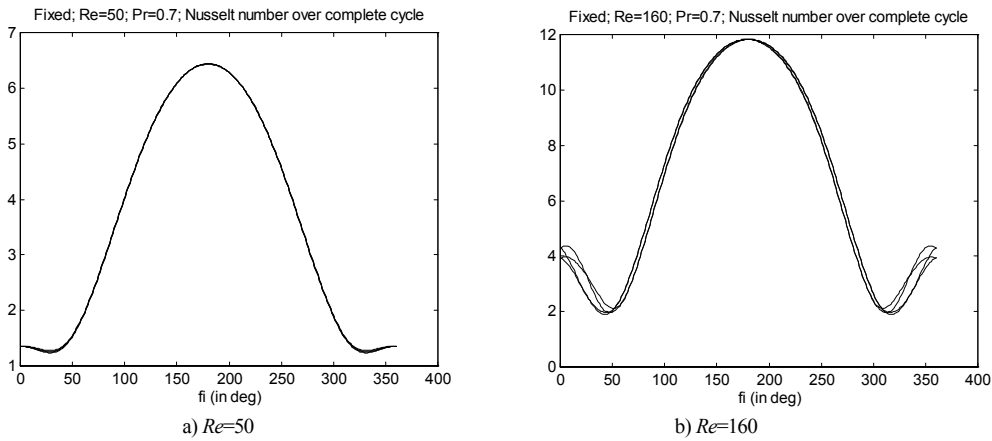

Figure 6. Time history of average Nusselt number

a) *Re*=50   b) *Re*=160

Figures 7a and b. Local Nusselt number

Figures 7a and 7b show the local Nusselt number distribution over the cylinder surface for a complete cycle of vortex shedding at dimensionless times t_0; $t_0 - \frac{T}{4}$; $t_0 - \frac{T}{2}$; $t_0 - \frac{3T}{4}$ where $t_0 = 250$ and T is the period of a shedding cycle. As can be seen, the curves are similar in shape and magnitude, but shift slightly over the whole periphery, and the shift is largest on the downstream side of the cylinder. At Re=50 the four curves belonging to the different phases almost completely coincide (Figure 7a), but the shift among the curves grows pronouncedly larger as the Reynolds number increases (see Figure 7b for an example). The maximum heat transfer rate is around φ =180°, near the upstream stagnation point. This can be attributed to the

thin boundary layer present at that point. As the boundary layer thickens, the local Nusselt number decreases steeply. The function seems to be completely symmetrical around this point, and minimum heat transfer occurs not at the exactly opposite downstream point, but around 45° to each side of it. There is a local maximum in the heat transfer at the downstream point ($\varphi = 0^o$), probably due to periodic vortex shedding.

The curves in Figures 7a and 7b are very similar to those based on computational results obtained using the stream function-vorticity method [8]. These researchers showed results for Re=200, a somewhat unfortunate choice as they used a two-dimensional code.

5. Concluding remarks

The finite difference method was applied for the numerical simulation of unsteady laminar flow and forced convection from a fixed cylinder placed in a uniform flow. Primitive variable formulation was used for the fluid flow, and the fluid is assumed to be incompressible and of constant property. The viscous energy dissipation term was neglected in the energy equation since its value is small at low Reynolds numbers. By using boundary-fitted coordinates, interpolation of the boundary conditions becomes unnecessary. An orthogonal transformation provides a fine grid scale in the vicinity of the cylinder and a coarse grid in the far field. Time derivatives are approximated by forward differences, space derivatives by fourth order central differences, except for convective terms which were approximated by a third order modified upwind scheme.

The code developed was applied to the investigation of both flow around a circular cylinder and forced convection from the cylinder. The non-dimensional vortex shedding frequency (Strouhal number), time-mean values of drag and of base pressure coefficients, further the root-mean- square values of lift, drag, base pressure, and Nusselt number were determined for Reynolds numbers from 50 to 180. Where possible, results were compared with experimental data and excellent agreement was obtained, except for the vicinity of Re=180, where three-dimensional instability might have had an influence.

The distribution of the local Nusselt number over the cylinder surface was also investigated over a complete cycle. It was found that the curves belonging to different phases are similar in shape and magnitude, but shift slightly over the whole periphery of the cylinder, and the shift is largest on the downstream side of the cylinder. This shift increases with increasing Reynolds number.

The good agreement found between experimental and computational values encourages the author to extend the investigation in the future to the cases of forced convection from an oscillating cylinder, and to the three-dimensional case. Another future plan is to take into account the effect of temperature on the properties of the fluid.

REFERENCES

1. ROSHKO, A.: *On the development of turbulent wakes from vortex streets*, NACA Rep., 1191, 1954.

2. NORBERG, C.: *Flow around a circular cylinder: aspects of fluctuating lift,* Journal of Fluids and Structures, **15**, (2001), 459-469.

3. BEARMAN, P.W.: *Developments in the understanding of bluff body flows,* JSME Centennial Grand Congress, International Conference on Fluid Engineering, **1**, Tokyo, (1997), 53-61.

4. KAWAMURA, T. and KUWAHARA, K. : *Computation of high Reynolds number flow around a circular cylinder with surface roughness*, Proceedings of the 22nd Aerospace Sciences Meeting, Reno, Nevada, AIAA-84-0340, (1984), 1-11.

5. BRAZA, M., CHASSAING, P. and MINH, H. H.: *Numerical study and physical analysis of the pressure and velocity fields in the near wake of a circular cylinder*, Journal of Fluid Mechanics, **165**, (1986), 79-130.

6. KARNIADAKIS, G.E. and TRIANTAFYLLOU, D.S.: *Frequency selection and asymptotic states in laminar wakes.* Journal of Fluid Mechanics, **199**, (1989), 441-469.

7. LANGE, C.F., DURST, F. and BREUER, M.: *Momentum and heat transfer from cylinders in laminar crossflow at $10^{-4} \leq Re \leq 200$,* International Journal of Heat and Mass Transfer, **41**, (1998), 3409-3430.

8. MAHFOUZ, F.M. and BADR, H.M.: *Forced convection from a rotationally oscillating cylinder placed in a uniform stream,* International Journal of Heat and Mass Transfer, **43**, (2000), 3093-3104.

9. BARANYI, L. and SHIRAKASHI, M.: *Numerical solution for laminar unsteady flow about fixed and oscillating cylinders*, Computer Assisted Mechanics and Engineering Sciences, **6**, (1999), 263-277.

10. ROSHKO, A.: *Perspective on bluff body aerodynamics*, Journal of Wind Engineering and Industrial Aerodynamics, **49**, (1993), 79-100.

11. HARLOW, F.H. and WELCH, J.E.: *Numerical calculation of time-dependent viscous incompressible flow of fluid with free surface*, Physics of Fluids, **8**, (1965), 2182-2189.

12. FLETCHER, C.A.J.: *Computational Techniques for Fluid Dynamics*, Vol. 2, Springer, 2nd Ed., Berlin, 1997.

13. WILLIAMSON, C.H.K.: *Vortex dynamics in the cylinder wake*, Annual Review of Fluid Mechanics, **28**, (1996), 477-539.

14. ÖZISIK, M.N.: *Heat Transfer, A Basic Approach,* McGraw-Hill, New York, 1985.

15. MCADAMS, W.H.: *Heat Transmission,* McGraw-Hill, New York, Third edition, 1954.